

Process Optimization for Lattice-Selective Wet Etching of Crystalline Silicon Structures

Ronald G. Dixon

National Institute of Standards and Technology, 100 Bureau Drive Gaithersburg, MD 20899-8212

Phone number: 301-975-4399

Fax: 301-869-0822

Email: ronald.dixon@nist.gov

William F. Guthrie

National Institute of Standards and Technology, 100 Bureau Drive Gaithersburg, MD 20899-8980

Phone number: 301-975-2854

Fax: N/A

Email: william.guthrie@nist.gov

Richard A. Allen

National Institute of Standards and Technology, 100 Bureau Drive Gaithersburg, MD 20899-8120

Phone number: 301-975-5026

Fax: 301-869-0822

Email: richard.allen@nist.gov

Ndubuisi G. Orji

National Institute of Standards and Technology, 100 Bureau Drive Gaithersburg, MD 20899-8212

Phone number: 301-975-3475

Fax: 301-869-8022

Email: ngorji@nist.gov

Michael W. Cresswell*

National Institute of Standards and Technology, 100 Bureau Drive Gaithersburg, MD 20899-8120

Phone number: N/A

Fax: N/A

Email: mcresswel@yahoo.com

Christine E. Murabito*

National Institute of Standards and Technology, 100 Bureau Drive Gaithersburg, MD 20899-8120

Phone number: N/A

Fax: N/A

Email: christine.murabito@gmail.com

*Present addresses unavailable. (Authors were with NIST during their involvement with this work, but are no longer affiliated with NIST.)

ABSTRACT

Lattice-selective etching of silicon is used in a number of applications, but it is particularly valuable in those for which the lattice-defined sidewall angle can be beneficial to the functional goals. A relatively small but important niche application is the fabrication of tip characterization standards for critical dimension atomic force microscopes (CD-AFMs).

CD-AFMs are commonly used as reference tools for linewidth metrology in semiconductor manufacturing. Accurate linewidth metrology using CD-AFM, however, is critically dependent upon calibration of the tip width. Two national metrology institutes (NMIs) and at least two commercial vendors have explored the development of tip calibration standards using lattice-selective etching of crystalline silicon.

The National Institute of Standards and Technology (NIST) standard of this type is called the single crystal critical dimension reference material (SCCDRM). These specimens, which are fabricated using a lattice-plane-selective etch on (110) silicon, exhibit near vertical sidewalls and high uniformity and can be used to calibrate CD-AFM tip width to a standard uncertainty of less than 1 nm.

During the different generations of this project, we evaluated variations of the starting material and process conditions. Some of our starting materials required a large etch bias to achieve the desired linewidths. During the optimization experiment described in this paper, we found that for KOH etching of the silicon features, it was possible to independently tune the target linewidth and minimize the linewidth non-uniformity. Consequently, this process is particularly well-suited for small-batch fabrication of CD-AFM linewidth standards.

Keywords: lattice-selective etching, crystalline silicon etching, CD-AFM, metrology, CD, linewidth, SCCDRM, standards, calibration

1. INTRODUCTION

Anisotropic, lattice-selective etching of silicon has been known and used in semiconductor manufacturing since the 1960s.[1] It has been used for a number of applications, but it is particularly valuable in those for which the lattice-defined sidewall angle can be beneficial to the functional goals.[2-5] The potential for deep etching of near-vertical sidewalls has also made it appropriate for micro-electromechanical systems (MEMS).[6-9] During the last 15 years a relatively small but important niche application in metrology has emerged: the fabrication of tip characterization standards for critical dimension atomic force microscopes (CD-AFMs).[10-13]

CD-AFMs use flared tips and two-axis surface sensing and tip control in order to image features with vertical and slightly reentrant sidewalls.[14-15] These instruments are commonly used as reference tools for linewidth metrology in semiconductor manufacturing. Accurate linewidth metrology using CD-AFM, however, is critically dependent upon calibration of the tip width.[16-17] Since the primary effect of CD-AFM tip-sample dilation is an additive bias of the measured width, the most effective method of tip calibration is to measure the apparent width of a known structure to determine the effective tip width.

Historically, many CD-AFM users have developed in-house reference standards for tip width calibration – often based on scanning electron microscope (SEM) or transmission electron microscope (TEM) cross sections. But the resultant uncertainty of such standards can be significant. Tip characterizer samples - which have a sharp ridge that can be used to calibrate tip width - are commercially available. However, scanning such samples can result in tip damage, and the standard uncertainty of tip calibrations based on this typically exceeds 5 nm.

Since the early 2000s, two national metrology institutes (NMIs), the National Institute of Standards and Technology (NIST) in the United States and the Physikalisch-Technische

Bundesanstalt (PTB) in Germany, and at least two commercial vendors have explored the development of standards suitable for CD-AFM tip calibration.[10-13,18] In most of these cases, lattice-selective etching of crystalline silicon was involved in the fabrication process.

The NIST standard of this type is called the single crystal critical dimension reference material (SCCDRM). These specimens, which are fabricated using a lattice-plane-selective wet etch on (110) silicon, exhibit near vertical sidewalls and high uniformity and can be used to calibrate CD-AFM tip width to a standard uncertainty of less than 1 nm.

During the different generations of this project, we experimented with different variations on the starting material and process conditions – including the etchant.[11,19] Both potassium hydroxide (KOH) and tetramethyl ammonium hydroxide (TMAH) are commonly used etchants. Some of our starting materials required a large etch bias to achieve the desired linewidths. During the optimization experiment described in this paper, we found that for KOH etching of the silicon features, it was possible to independently tune the target linewidth and minimize the linewidth non-uniformity. Consequently, this process is particularly well-suited for small-batch fabrication of CD-AFM tip calibration standards.

2. SCCDRM ETCH PROCESS OPTIMIZATION EXPERIMENT

The background and overall methodology of the SCCDRM project has been described elsewhere.[10-11] While we have experimented with differences in the starting material and processing, the use of selective etching on (110) Si has always been a key element. For some generations of the project, we used starting material with a buried oxide that served both as an etch stop and as an electrical isolation layer. In this paper, we are specifically dealing with etch

optimization experiments using silicon-on-insulator (SOI) starting material that itself was fabricated using an implantation process – such as separation by implantation of oxygen (SIMOX).

In figure 1, we illustrate some of the major characteristics of the current starting material and process. The substrate and device layer – in which the features are patterned – are both (110) crystalline silicon and are separated by a buried oxide. The device layer was approximately 160 nm thick and the buried oxide was about 390 nm. This same type of starting material was also used in prior generations of the SCCDRM [11,19] – including the first one to combine the use of CD-AFM and HRTEM for the calibration.[10]

For small-batch fabrication projects like the SCCDRMs, access to suitable lithography at affordable costs can be a challenge. The trade-offs between electron beam direct write lithography and optical lithography present challenges either way. Electron beam lithography offers very small resolution, avoids the cost of mask making, and does not require large batches or even whole wafers. However, the cost is generally proportional to write time and thus essentially proportional to the patterned area. This makes it most suitable for samples on which the patterned region is a relatively small percentage of the surface area.

Optical lithography, on the other hand has much higher throughput and lower cost for patterned area, but significantly worse resolution and a large one-time cost of mask fabrication. The minimum sensible batch size would correspond to a whole wafer – with those associated costs. For applications in which the lithography resolution is not a limiting factor (e.g., when an etch bias can be used to achieve the desired feature width) and the mask costs are affordable, the advantages of optical lithography probably outweigh those of electron beam lithography. Ultimately, we used *i*-line (365 nm) lithography for most generations of the SCCDRMs and for the starting material used in this etch optimization experiment.

The typical hard mask thickness is about 10 nm. In some of our earlier experiments, a silicon nitride hard mask was used because nitride has greater resistance to the selective etch step. However, the post etch removal of a nitride mask is significantly more difficult than the removal of an oxide. In some prior experiments, particles or residue from the hard mask remained on the final features. Therefore, we used an oxide hard mask for SCCDRM production and for the current optimization experiment.

Following the lithography and pattern transfer to the hard mask, the wafers were diced into individual chips for the remainder of the process. A lattice-plane-selective etch is then used to define the features in the device layer. During some generations of this project, both tetramethyl ammonium hydroxide (TMAH) and potassium hydroxide (KOH) were evaluated as etchants.

For previous production generations of SCCDRMs, the etchant used was TMAH.[11,19] This was motivated largely by the use of an oxide hard mask which has a greater resistance to TMAH than to KOH. For the current process optimization experiment, however, we used a KOH etch – which has a larger relative lattice-plane selectivity than TMAH and offers the potential for a greater etch bias.

2.1 Design of Etch Optimization Experiment

The final feature characteristics of the SCCDRM will have some dependence on both the properties of the starting material and performance of the lithography. However, it is the lattice-selective etch that is central to functional application of the features. Since the wafers were diced into individual chips after the lithography, it is also possible to readily vary the etch parameters on a chip by chip basis. More importantly, our overall technical objectives were to reduce feature size and CD non-uniformity, and we believe that these characteristics have a greater sensitivity to the

etch conditions than to the details of the initial lithography. The etch-related factors were thus the focus for this optimization experiment.

Barring major defects in crystallinity of the device layer or on the mask pattern, we would expect the selective etch to smooth out most of the width non-uniformity of the features due to imperfections in the mask or the lithography step. But the extent to which this is accomplished will depend on how closely the etch conditions correspond to an idealized model. In addition to the primary etch conditions, we also incorporated cleaning factors into the experiment. Although the cleaning process is not the central issue in fabrication of SCCDRMs, the removal of both particulates and hydro-carbon deposition from scanning electron microscope (SEM) inspection were of concern during the project.

The overall process optimization experiment employed a model with six two-level factors in a 2^{6-2} or quarter-replicate design. This method allows for estimation of all main effects and some two-factor interactions from only 16 runs instead of the 64 that would be required in a full factorial design.[20]

The six factors were:

1. Pre-thinning of the oxide hard mask before silicon patterning,
2. Concentration of KOH and etch duration used for patterning,
3. Use of ultrasonic agitation during patterning,
4. Use of ultrasonic agitation during cleaning of chips with iso-propyl alcohol,
5. Duration of cleaning with iso-propyl alcohol, and
6. Use of acetone or acetone and gaseous ozone to remove carbon deposits following SEM inspection.

The inclusion of a post-SEM cleaning step as factor 6 served to support the goals of using SEM inspection on the SCCDRMs during process development. The observed effects of factor 6 would allow us to evaluate the performance of the SCCDRMs under SEM inspection and the consequent importance of the cleaning process for potential contamination. However, our emphasis here is on the application of SCCDRMs for CD-AFM tip calibration. Since SEM inspection and cleaning is not required for this purpose, most of our analysis and discussion will be limited to the first five factors. As shown in table I, this scope reduction results in a model with five two-level factors in a 2^{5-1} or half-replicate design.

The process flow generally follows the order of the factors above and from left to right across the columns in table I. However, factors 2 and 3 pertain to the same process step – the lattice-selective silicon etch – and thus occur simultaneously. This is also true of factors 4 and 5 – which describe the cleaning step after patterning. Note also that factor 1 has a complementary process step – the hard mask strip – which is shown in table I, but which is not treated as an independent factor. This is because the total etch time using the buffered oxide etch (BOE) is held constant at 18 seconds – which was determined to be sufficient to remove all of the oxide. Therefore, the variable described by factor 1 indicates whether the oxide mask is stripped in one step following the lattice-selective silicon etch, or in two steps including a pre-thinning.

Optical inspection, when necessary to verify chip condition, was performed on the chips during the process steps involving the first five factors. At that point, CD-AFM measurements were performed to determine the linewidth and non-uniformity of the target features. Then an SEM inspection was performed and the final cleaning step (factor 6) was completed. The CD-AFM measurements were performed at NIST, but the SEM measurements were performed by an external supplier.

The SCCDRM chips have a large number of features on them, and the measurement of all of them by either AFM or SEM would be prohibitive. For this experiment we focused on the variable linewidth grid (VLG) targets. Each VLG target consists of an array of six lines of different designed linewidths. A top-down SEM image of a VLG target is shown in figure 2, and a CD-AFM image of a VLG target is shown in figure 3. Note that the orientation of the target differs by 90° between the images since CD-AFM data is typically rendered with the horizontal image axis corresponding to the fast scan axis. This type of target has both processing and metrology benefits. For processing purposes, this design provided a means of checking how the measured and designed widths tracked locally independent of spatial variations in etching or material. For metrology purposes, these targets allowed the incorporation of a scale linearity test into the CD-AFM tip width calibration. The VLG targets are also referred to as high resolution transmission electron microscopy (HRTEM) targets, because they were used for both the HRTEM transfer and the final calibration steps using CD-AFM.[10]

For the first phase of AFM measurements, which was performed after the process steps corresponding to the first five factors, we selected two types of target on each chip. One was the smallest design-width target that had all six features intact, and was, in general, different for every chip. This choice was necessary to assess the factor effects on minimum linewidth. The second target measured on each chip was one with the largest design-width – which was always the same. This choice would potentially allow us to detect any influence related to defects in the mask, and it also provides independent confirmation of the factor effects on non-uniformity determined from the measurements of the smallest design-width targets.

Following the first phase of AFM measurements, the SEM measurements were performed only on the smallest surviving design-width targets. An AFM re-check of selected targets was then

performed to assess the level of hydrocarbon contamination deposited by the SEM. A typical level of contamination is a few nanometers thick.

The last cleaning step, described by factor 6, was used to remove any contamination deposited during the SEM inspection. Although alternative cleaning processes may be explored in the future, we decided to compare an acetone clean with an acetone and ozone clean for this factor. Following the final clean, those features that had been measured by SEM were measured again using the AFM.

2.2 Analysis of Results

We analyzed the CD-AFM data to determine the sensitivity of two feature characteristics to the experimental factors. These characteristics were the minimum linewidth and linewidth non-uniformity. To quantify the non-uniformity, we used a metric that was developed as part of our uncertainty analysis for using CD-AFM to transfer the HRTEM calibration to other samples. Essentially, this metric involves the use of a triangular weighting function over the central 0.5 μm of the AFM data set – or 20 line scans – to calculate an average and standard uncertainty of the linewidth in that region. (Note that in figure 3, this region corresponds to 25 % of the image centered on the ‘tip’ of the navigation marker that is visible to the side.) This choice was motivated by our treatment of TEM/AFM relative positioning uncertainty when using CD-AFM in concert with HRTEM, and the details have been previously published.[10-11]

In figures 4 and 5 the factor effects plots for minimum linewidth and non-uniformity are shown. Only the effects of the first five factors are included in these plots, because these results were calculated from the initial AFM measurements (i.e., pre-SEM) taken on the smallest surviving target on each chip. We note, however, that the results taken from the largest design width target on

each chip lead to a substantively similar conclusion. This means that, as expected, there is no significant dependence on the specific target selected.

As the factor effects plots reveal, the minimum linewidth that survived etching is sensitive primarily to pre-thinning the hard mask and has little dependence on the remaining factors. This is physically reasonable since the narrowest features will be quickly undercut during oxide etch which strips the hard mask. Consequently, removing as much hard mask as possible up front can be expected to increase the survival of narrow lines. Additionally, it must be remembered that the hard mask is not totally immune to the KOH etch. The etch rate of the silicon is expected to be two to three orders of magnitude larger than the etch rate of the oxide hard mask. However, we did not experimentally verify this. And it is possible that once the hard mask is sufficiently pre-thinned, the effective lateral etch rate of the KOH on the oxide is sufficient to decrease the ultimate width of the resultant features. This also favors narrow lines and is consistent with our observations.

The non-uniformity has sensitivity to several factors and two-factor interactions, but very little sensitivity to pre-thinning of the hard mask. However, the single largest sensitivity is to the etchant concentration and etch time factor. This is also physically reasonable since we believe that local variations in the etch environment (e.g. concentration gradients) are a significant contributor to the observed non-uniformity of the final features. A lower etchant concentration applied for a longer period of time is more likely to result in average etch conditions that are more uniform and may thus be expected to produce structures with lower non-uniformity. This conclusion is consistent with our experimental observations.

Plots taken from the CD-AFM measurements of the least and most uniform process configurations are shown in figures 6 and 7. These figures illustrate the variation in measured linewidth for each of the 80 scan lines that comprise each image – such as the example in figure 3.

The plots illustrate results of the best and worst process conditions observed in the experiment. As can be seen in figure 7, we were able to achieve linewidths as low as 20 nm. The standard uncertainty due to non-uniformity in the central 0.5 μm section of that feature, as defined by the metric previously described, is 0.45 nm.

In figures 8 and 9 the normal probability plots are shown for both minimum linewidth and non-uniformity. These plots were also based only the first five factors and the CD-AFM results on the smallest width target prior to SEM inspection. The figures clearly demonstrate that statistically significant conclusions can be drawn from the factor effects plots. Although the minimum CD has some statistically significant dependence on two two-factor interactions, both of these involve pre-thinning of the hard mask – which is the only factor that has a significant main effect – a dependence we believe is well understood.

The non-uniformity exhibits a statistically significant dependence on two factors and one two-factor interaction. As discussed above, the importance of the factor for etchant concentration and etch time is not surprising, and the effect of ultra-sonic cleaning is also not unreasonable – particularly considering that some of the apparent non-uniformity is probably due to residue on the features. However, the significant dependence of the non-uniformity on the two-factor interaction between ultra-sonic etch and cleaning duration is not fully understood. Further investigation of significant effects identified in this experiment would be valuable, but we can conclude from these results that this type of process is very well suited for applications such as CD-AFM tip calibration standards.

3. SUMMARY AND PLANS

An important niche application of lattice-selective wet etching of silicon is the fabrication of tip characterization standards for critical dimension atomic force microscopes (CD-AFMs). Since accurate linewidth metrology using CD-AFM is critically dependent upon calibration of the tip width, all applications of CD-AFM metrology are ultimately dependent upon tip calibration. At least two NMIs have developed tip calibration standards for CD-AFM using lattice-selective etching of silicon.

The NIST standard of this type is called the single crystal critical dimension reference material (SCCDRM). These specimens, which are fabricated using a lattice-plane-selective etch on (110) silicon, exhibit near vertical sidewalls and high uniformity and can be used to calibrate CD-AFM tip width to a standard uncertainty of less than 1 nm.

In this paper we described an optimization experiment for the KOH etching of silicon features such as those on the SCCDRMs. The results showed that it was possible to independently tune the target linewidth and minimize the linewidth non-uniformity. We observed minimum feature sizes of 20 nm and non-uniformity of less than 1 nm. Consequently, this process is particularly well-suited for small-batch fabrication of CD-AFM tip calibration standards.

For potential refinement experiments in the future, we are considering other levels of the etch factor and alternative cleaning processes which were considered too aggressive for the current experiment. The so-called ‘piranha’ clean, which uses a mixture of sulphuric acid (H_2SO_4) and hydrogen peroxide (H_2O_2), is one candidate. This cleaning process is commonly used in the micro-electro-mechanical systems (MEMS) industry to remove resist and other organic residue.[21]

ACKNOWLEDGEMENTS

This work was supported by the Engineering Physics Division of the NIST Physical Measurement Laboratory (PML).

*Address all correspondence to Ronald Dixson at ronald.dixson@nist.gov

†Certain commercial equipment is identified in this paper to adequately describe the experimental procedure. Such identification does not imply recommendation or endorsement by the National Institute of Standards and Technology nor does it imply that the equipment identified is necessarily the best available for the purpose.

REFERENCES

1. D. B. Lee, "Anisotropic etching of silicon," *J. Appl. Phys.* **40** (11), 4569-4574 (1969).
2. K. E. Bean, "Anisotropic etching of silicon," *IEEE Trans. Electron Dev.* **25** (10), 1185-1193 (1978).
3. D. L. Kendall, "Vertical etching of silicon at very high aspect ratios," *Ann. Rev. Mater. Sci.* **9**, 373-403 (1979).
4. H. Seidel et al., "Anisotropic etching of crystalline silicon in alkaline-solutions 1. Orientation dependence and behavior of passivation layers," *J. Electrochem. Soc.* **137** (11), 3612-3626 (1990).
5. E. S. Ammar and T. J. Rodgers, "UMOS transistors on (110) silicon," *IEEE Trans. Electron Dev.* **27** (5), 907-914 (1980).
6. E. Bassous and E. F. Baran, "Fabrication of high precision nozzles by anisotropic etching of (100) silicon," *J. Electrochem. Soc.* **125**, 1321-1327 (1978).
7. S. K. Clark and K. D. Wise, "Pressure sensitivity in anisotropically etched thin-diaphragm pressure sensors," *IEEE Trans. Electron Dev.* **26**, 1887-1896 (1979).

8. P. L. Chen, R. S. Muller, R. D. Jolly, G. L. Halac, R. M. White, A. P. Andrews, T. C. Lim, M. E. Motamedi, "Integrated silicon microbeam PI-FET accelerometer," *IEEE Trans. Electron Dev.* **29**, 27-33 (1982).
9. K. E. Peterson, A. Shartel, N. F. Raley, "Micromechanical Accelerometer Integrated with MOS Detection Circuitry," *IEEE Trans. Electron Dev.* **29**, 23-27 (1982).
10. R. G. Dixon, R. A. Allen, W. F. Guthrie, and M. W. Cresswell, "Traceable Calibration of Critical-Dimension Atomic Force Microscope Linewidth Measurements with Nanometer Uncertainty," *J. Vac. Sci. Technol. B* Vol. **23**, 3028-3032 (2005).
11. M. Cresswell, W. Guthrie, R. Dixon, R. A. Allen, C. E. Murabito, J. V. Martinez de Pinillos, "RM8111: Development of a Prototype Linewidth Standard," *J. Res. Natl. Inst. Stand. Technol.* **111**, 187 – 203 (2006).
12. G. Dai, M. Heidelmann, C. Kübel, R. Prang, J. Fuegge, and H. Bosse, "Reference nano-dimensional metrology by scanning transmission electron microscopy," *Meas. Sci. Technol.* **24**, 085001 (2013).
13. G. Dai, F. Zhu, M. Heidelmann, G. Fritz, T. Bayer, S. Kalt, J. Fluegge, "Development and characterisation of a new linewidth reference material," *Meas. Sci. Technol.* **26**, 115006 (2015).
14. Martin, H. K. Wickramasinghe, "Method for Imaging Sidewalls by Atomic Force Microscopy," *Applied Physics Letters* **64**, 2498-2500 (1994).

15. I. Schmitz, M. Osborn, S. Hand, Q. Chen, "Improvement in metrology on new 3D-AFM platform," *SPIE Proceedings* Vol. **7122**, 71222X (2008).
16. N. G. Orji, R. G. Dixson, A. Martinez, B. D. Bunday, J. A. Allgair, and T. V. Vorburger, "Progress on implementation of a reference measurement system based on a critical-dimension atomic force microscope," *J. Micro/Nanolith. MEMS MOEMS* Vol. **6**, 023002-1-10 (2007).
17. R. Dixson, N. G. Orji, C. D. McGray, J. Bonevich, J. Geist, "Traceable Calibration of a Critical Dimension Atomic Force Microscope," *J. Micro/Nanolith. MEMS MOEMS* Vol. **11**, 011006 (2012).
18. M. Tortonese, G.F. Lorusso, R.M. Blanquies, J. Prochazka, L. Grella, "Sub-50-nm isolated line and trench width artifacts for CD metrology," *SPIE Proceedings* Vol. **5375**, 647-656 (2004).
19. M. W. Cresswell, E. H. Bogardus, J. V. Martinez de Pinillos, M. H. Bennett, R. A. Allen, W. F. Guthrie, C. E. Murabito, B. A. am Ende, L. W. Linholm, "CD Reference Materials for Sub-Tenth Micrometer Applications," *SPIE Proceedings* Vol. **4689**, 116 - 127 (2002).
20. G. E. P. Box, W. G. Hunter, J. S. Hunter, "Statistics for Experimenters: An Introduction to Design, Data Analysis, and Model Building," Wiley-Interscience; 1st edition June 22 (1978).
21. C. A. Savran, A. W. Sparks, J. Sihler, J. Li, W. Wu, D. E. Berlin, T. P. Burg, "Fabrication and characterization of a micromechanical sensor for differential detection of nanoscale motions," *Journal of Microelectromechanical Systems*, Vol. **11**, 703 - 708, (2002).

Table I. Details of the SCCDRM process optimization experiment. For the 16 different experimental treatments labeled as A through P, there were two chips processed at each condition. The table shows the details of the treatments for the first five of the six two-level factors used in the experiment. Factor 6 is the type of cleaning (acetone or ozone) used after an SEM inspection, but it is not shown in the table because it is not central to etch optimization. The overall experiment is a 2^{6-2} fractional design with respect to all six factors. This method allows estimation of all main effects and some two-factor interactions. (Note that the hard mask removal step is not an independent factor but a complementary process step to factor 1 – since total BOE time is fixed at 18 s.)

Process Step:	<i>Pre-Thin Hard Mask (BOE)</i>	<i>Etchant Concentration and Etch Time</i>	<i>Ultrasonic Agitation During Etch</i>	<i>Hard Mask Removal (BOE)</i>	<i>Ultrasonic Agitation During IPA Cleaning</i>	<i>Duration of IPA Cleaning</i>	
Factor #	<i>1</i>	<i>2</i>	<i>3</i>	<i>1*</i>	<i>4</i>	<i>5</i>	
Experimental Treatments (A thru P)	A	No	25 % KOH/25 s	No	18 s	No	30 s
	B	10 s	25 % KOH/25 s	No	8 s	No	100 s
	C	No	25 % KOH/25 s	No	18 s	Yes	100 s
	D	10 s	25 % KOH/25 s	No	8 s	Yes	30 s
	E	No	12.5 % KOH/35s	No	18 s	No	100 s
	F	10 s	12.5 % KOH/35s	No	8 s	No	30 s
	G	No	12.5 % KOH/35s	No	18 s	Yes	30 s
	H	10 s	12.5 % KOH/35s	No	8 s	Yes	100 s
	I	No	25 % KOH/25 s	Yes	18 s	No	30 s
	J	10 s	25 % KOH/25 s	Yes	8 s	No	100 s
	K	No	25 % KOH/25 s	Yes	18 s	Yes	100 s
	L	10 s	25 % KOH/25 s	Yes	8 s	Yes	30 s
	M	No	12.5 % KOH/35s	Yes	18 s	No	100 s
	N	10 s	12.5 % KOH/35s	Yes	8 s	No	30 s
	O	No	12.5 % KOH/35s	Yes	18 s	Yes	30 s
	P	10 s	12.5 % KOH/35s	Yes	8 s	Yes	100 s

FIGURE CAPTIONS

Figure 1: Schematic of SOI starting material and SCCDRM process. For both prior generations and current experiment, the device layer is approximately 160 nm thick and the buried oxide is about 390 nm. The typical hard mask thickness is about 10 nm. Although earlier experiments used a silicon nitride hard mask, oxide was used for both SCCDRM production and this optimization experiment. The etchant used for this work was KOH.

Figure 2: Top down SEM image of an SCCDRM VLG target – as used for the HRTEM calibration transfer to CD-AFM and also as the test target in the optimization experiment.

Figure 3: Wire-frame rendering of CD-AFM image of an SCCDRM VLG target similar to the one in Figure 2. Note the apparent 90° rotation, because the fast scan axis is rendered horizontally, and that a portion of the navigation marker is visible to the side of the image.

Figure 4: Factor effects plot for minimum linewidth. The most important single factor effect is pre-thinning of the oxide hard mask prior to the silicon etch. (Notes: (1) Common background color indicates confounded effects; (2) factor six is not included.)

Figure 5: Factor effects plot for linewidth non-uniformity. The most important single factor effect is the etchant concentration and time. (Notes: (1) Common background color indicates confounded effects; (2) factor six is not included.)

Figure 6: Example of CD-AFM data on feature from worst process condition. The plot shows the linewidth calculated from individual linescans taken along a 2 μm length of the feature. The orange curve indicates the portion of data used to calculate the non-uniformity metric.

Figure 7: Example of CD-AFM data on feature from best process condition. The plot shows the linewidth calculated from individual linescans taken along a 2 μm length of the feature. The orange curve indicates the portion of data used to calculate the non-uniformity metric.

Figure 8: Normal probability plot for factor effects on minimum linewidth showing the dramatic dependence on pre-thinning of the hard mask (factor 1) and statistical significance of the observation. (The numbers next to the data points indicate the associated factor or factors for two-factor interactions.)

Figure 9: Normal probability plot for factor effects on linewidth non-uniformity showing the statistical significance of three effects with the largest being the factor for etch time and etchant concentration (factor 2). (The numbers next to the data points indicate the associated factor or factors for two-factor interactions.)

Ronald Dixson is a physicist in the Physical Measurement Laboratory (PML) of the National Institute of Standards and Technology (NIST). His current research interests are calibration methods, traceability, and uncertainty analysis in atomic force microscope (AFM) dimensional metrology – including the NIST traceable AFM (T-AFM) project and metrology applications of critical dimension AFM (CD-AFM). He holds a Ph.D. in Physics and is a member of SPIE, AVS, and the American Physical Society.

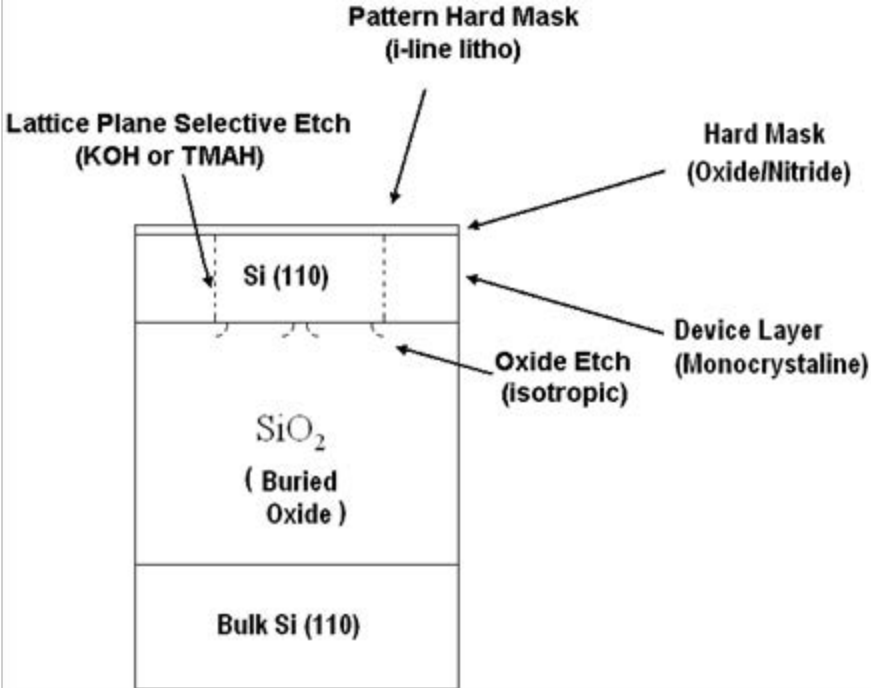
William F. Guthrie has been a statistician in the Statistical Engineering Division at NIST for the last 26 years, and he is currently serving as the Chief of that division. He collaborates with NIST researchers in a wide range of areas including semiconductor and microelectronics applications, building materials applications and chemical science applications. His statistical interests include design of experiments, uncertainty assessment, calibration, modern regression methods, Bayesian statistics, and statistical computation. He holds a B.A. in Mathematics from Case Western Reserve University and an M.S. in Statistics from the Ohio State University at Columbus.

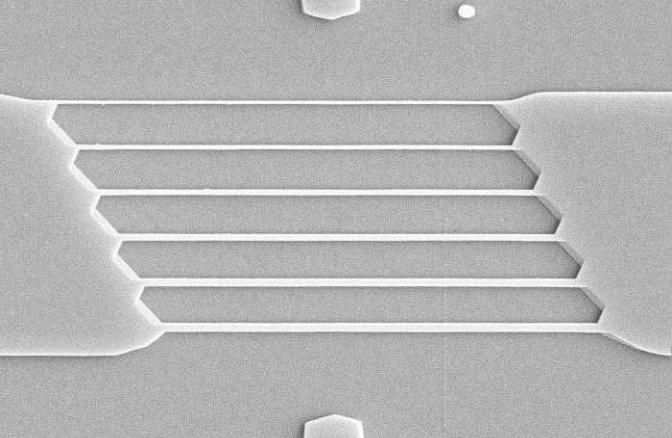
Richard A. Allen is a Physicist in the Engineering Physics Division at NIST, where his research areas are microdevices, motion metrology, and methods for calibration of accelerometers. He is a Co-Chair of the SEMI 3DS-IC Standards Committee and was NIST assignee to SEMATECH's 3D Enablement Center from 2011-2013. Mr. Allen received the B.S. and M.S., both in Physics, from Rensselaer Polytechnic Institute and his M.B.A. from Columbia Union College.

Ndubuisi G. Orji is a mechanical engineer in the Physical Measurement Laboratory of the National Institute of Standards and Technology (NIST). His research interests are in atomic force microscopy, surface metrology, nano-scale dimensional metrology, and optical metrology. He holds a PhD in mechanical engineering from the University of North Carolina at Charlotte. He is a

Michael W. Cresswell served for 19 years as a Senior Engineer at NIST in the former Electronics and Electrical Engineering Laboratory (EEL) – now part of the Physical Measurement Laboratory of the National Institute of Standards and Technology (NIST) and continued to serve as a contractor for five subsequent years. His research interest was developing methods for micro-machining crystalline structures to serve as reference materials for nanometer-scale critical-dimension metrology. He holds a PhD in physics from the Pennsylvania State and served a member of the American Physical Society. He is also a life-member of the Institute of Electrical and Electronic Engineers.

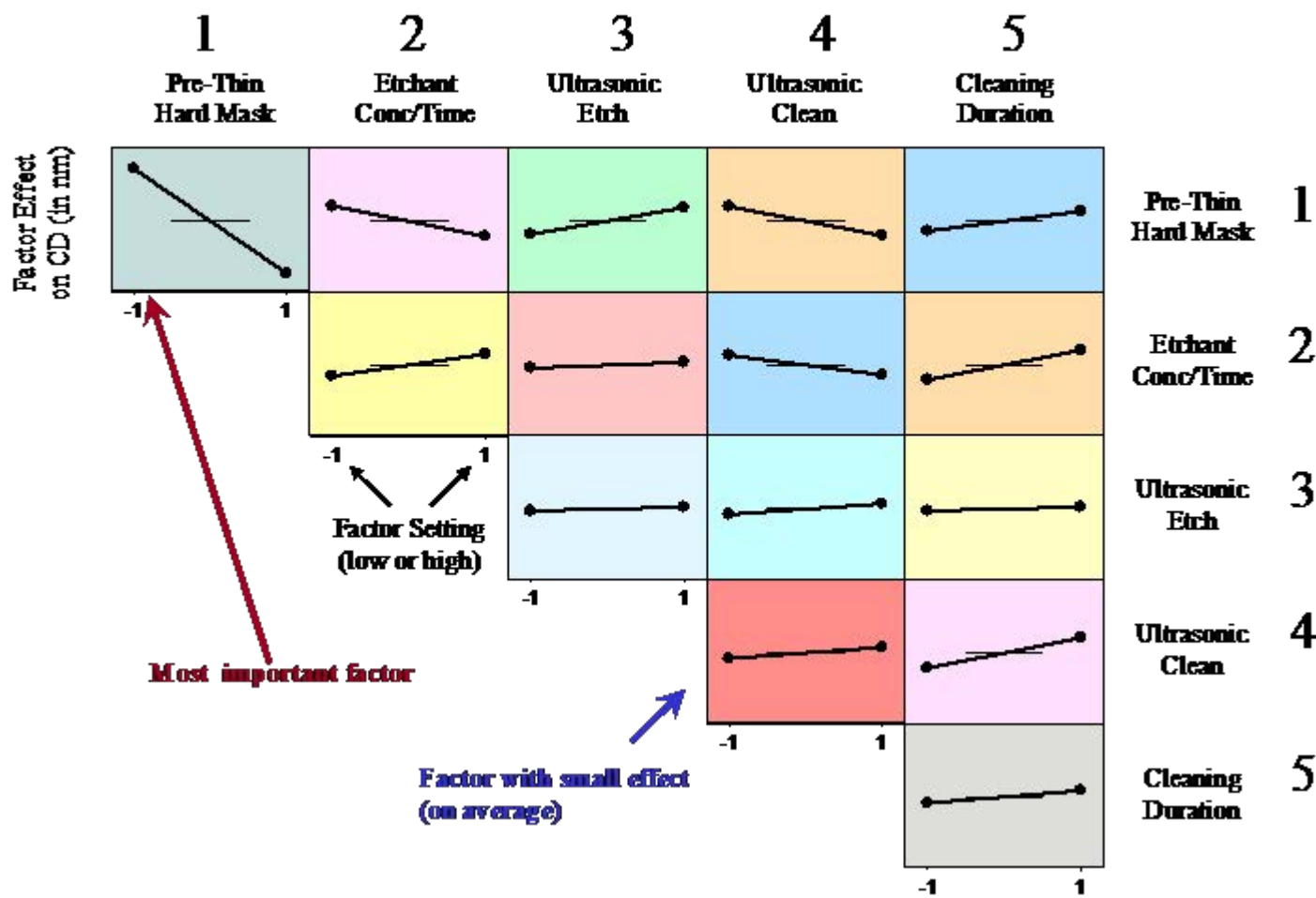
Christine E. Murabito– bio unavailable



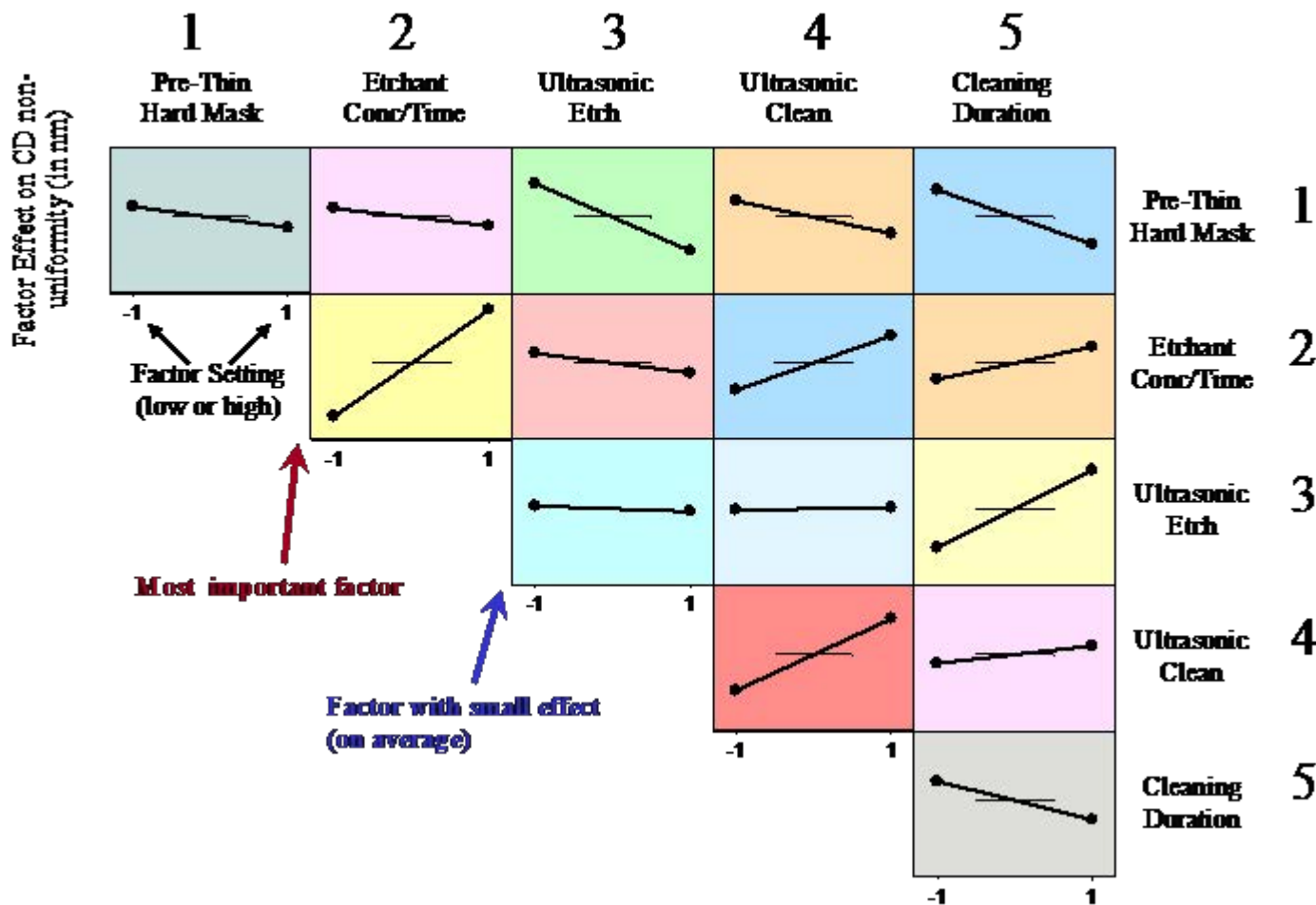


E-Beam	Det	Mag	HFW	Spot	Tilt	FWD	2 μm
10.0 kV	CDM-E	10.0 kX	15.2 μm	3	0.0°	4.921	B1

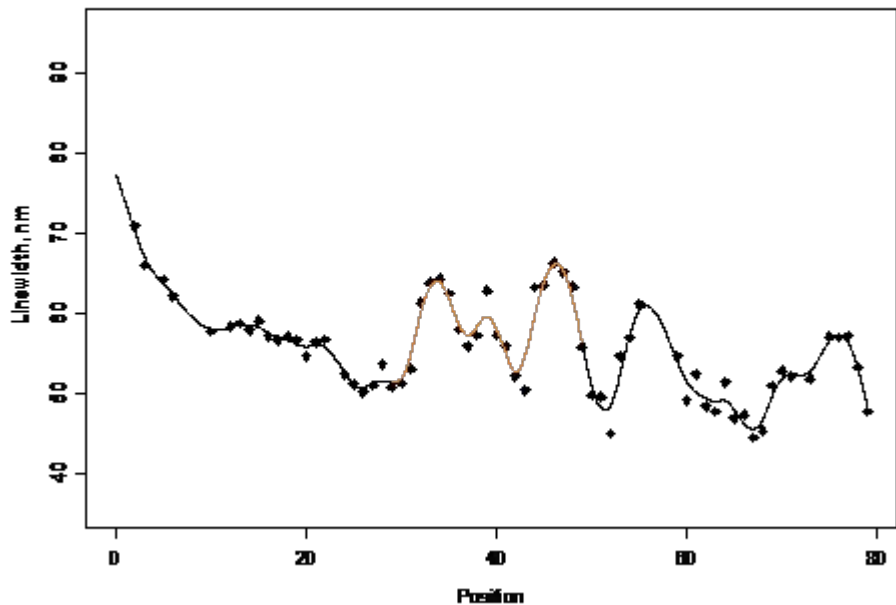
Effects Plots for Minimum CD



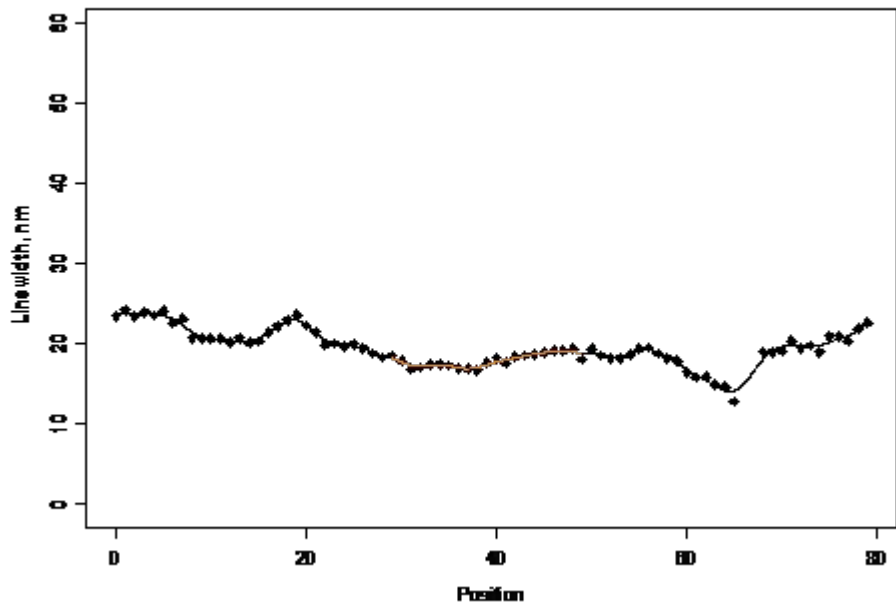
Effects Plots for CD Non-Uniformity



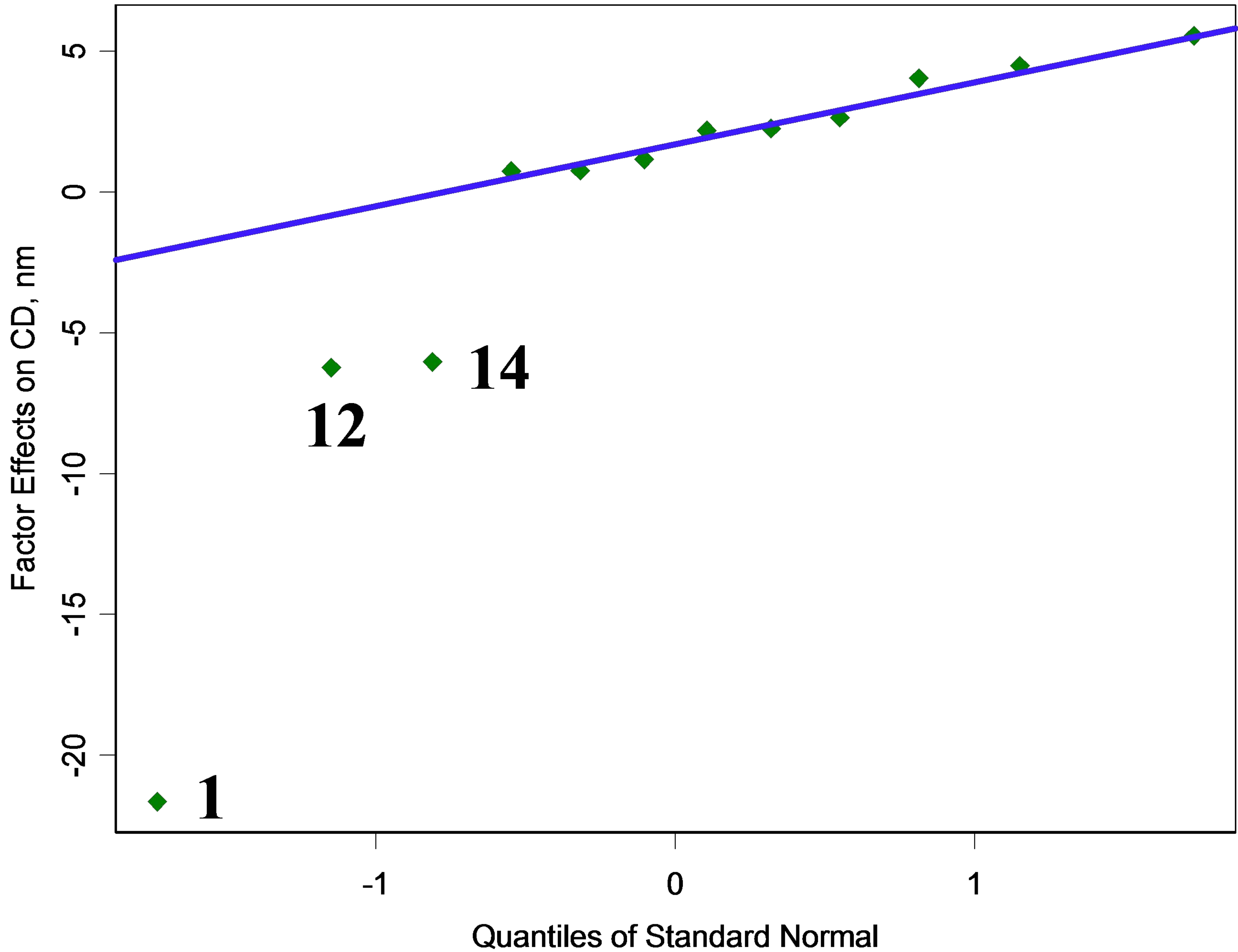
X12.K1.5p2T4-Feature 2 $\sigma(\text{Non-Uniformity}) = 3.01 \text{ nm}$



X12.H1.9p3T1- Feature 2: $\sigma(\text{Non-Uniformity}) = 0.45 \text{ nm}$



CD



Non-Uniformity

